Chemical Science

ROYAL SOCIETY OF CHEMISTRY

EDGE ARTICLE

View Article Online
View Journal



Cite this: DOI: 10.1039/d5sc06657c

All publication charges for this article have been paid for by the Royal Society of Chemistry

# Electronic and energy descriptors for SACs as tri-functional catalysts towards urea formation and unveiling the C–N coupling mechanism

Narad Barman,[a] Chiranjib Majumder[b] and Ranjit Thapa *[ac]

Single atom catalysts (SACs) have rapidly emerged as a cutting-edge trend in electro-catalysis for synthesizing nitrogen-based products such as ammonia, nitric acid and urea. In the present study, we considered $NO_2^-$ as a specific N-based molecule, which participated in the simultaneous reduction with $CO_2$ towards urea formation for 77 SACs. Our investigation demonstrates that among possible nitrogen-containing intermediates generated during the simultaneous electrochemical reduction of $CO_2$ and $NO_2^-$, only the $NH_2$ intermediate effectively couples with CO to form urea. In the case of simultaneous reduction towards urea formation, the $NH_2$ free energy serves as an effective energy descriptor for identifying suitable catalysts, exhibiting a strong linear correlation with the limiting potential ($R^2 = 0.93$). Additionally, we observed a strong Brønsted–Evans–Polanyi (BEP) relationship ($R^2 = 0.99$) between the $NH_2$ adsorption energy and the activation energy of the coupling intermediate ($CONH_2$). Furthermore, the out of plane d-sub orbitals ($d_{xz}$, $d_{yz}$ and $d_{z^2}$) of the transition metal (TM) were analysed to uncover the electronic origins of urea reactivity. Owing to the strong interaction between the d-sub orbitals of the TM and the $sp^3$ hybrid orbitals of $NH_2$, occupancy of the $d_{yz}$ orbitals plays a significant role in determining catalytic activity. This is evidenced by a linear correlation ($R^2 = 0.73$) between orbital occupancy of $d_{yz}$ and $NH_2$ adsorption energy for all systems, identifying it as the electronic origin of urea reactivity. Our interpretation regarding the descriptor is that $NH_2$ $sp^3$ (HOMO) donates a σ-electron to the TM d-orbital (LUMO), while the TM d-orbital (HOMO) donates a π*-electron back to $NH_2$ $sp^3$ (LUMO).

Received 29th August 2025
Accepted 19th November 2025

DOI: 10.1039/d5sc06657c

rsc.li/chemical-science



## Introduction

In the agricultural sector, urea serves as a nitrogen-rich (46%) fertilizer, enabling food production that sustains nearly 27% of the world's population.[1] Not only as an agricultural fertilizer, its chemical uses in numerous chemical products as feedstock make it invaluable.[1,2] At present, the energy-intensive Bosch–Meiser process is followed for the industrial production of urea ($NH_3 + CO_2 \rightarrow NH_2CONH_2 + H_2O$), (temperature >180 °C and pressure ≡ 150 bar) emitting large amounts of $CO_2$.[3,4] In stark contrast, synthesis of urea from $CO_2$ and other alternative N-sources such as $N_2$, $NO_3^-$, $NO_2^-$ *etc.* using an electrochemical cell under ambient conditions complies with sustainability goals.[5] But, the occurance of many side reactions such as the hydrogen evolution reaction (HER), $CO_2$ reduction reaction ($CO_2$RR) and $NO_3^-$ reduction reaction ($NO_3^-$RR) poses a significant challenge in the electrochemical synthesis of urea.[6–9] Thus, developing catalysts capable of reducing $CO_2$ and nitrogen-containing species while inhibiting the HER is of critical importance.

To overcome this problem, transition metal-based single-atom catalysts (TM-SACs) have shown significant potential, as they possess superior activities for the electrocatalytic $CO_2$RR, NRR, $NO_2$RR, and $NO_3$RR, while their activity towards the HER remains relatively low. Since 2011, first reported by Zhang *et al.*,[10] single atom catalysts (SACs) have become a hot topic for various electrocatalytic reactions such as the HER,[11,12] OER,[13–15] NRR[16–18] and $CO_2$RR,[19–22] due to their unique metallic design and superior catalytic performance.[10,23] Both theoretical and experimental studies point out that the transition metal (TM) centre in TM–N–C SACs is the possible active site for the $CO_2$RR and $NO_2$RR. Some studies suggest that single atom catalysts not only can reduce one molecule, but also reduce simultaneously $CO_2$ and N-based molecules ($N_2$, $NO_2^-$, and $NO_3^-$). For example, (i) Shibata *et al.* reported that TM–Pc SACs could simultaneously reduce $CO_2$ and nitrite ions towards formation of urea,[24] (ii) Ghorai *et al.* showed recently that Co–Pc supported on $MoS_2$ could co-reduce $N_2$ and $CO_2$ to form urea,[9] and (iii) recently Cheng *et al.* explored whether metal-$N_4$-functionalized graphene can co-reduce $NO_3^-$ and $CO_2$ towards urea formation *etc.*[25]

[a]*Department of Physics, SRM University AP, Amaravati 522240, Andhra Pradesh, India. E-mail: ranjit.phy@gmail.com*

[b]*Chemistry Division, Bhabha Atomic Research Centre Trombay, Mumbai 400 085, India*

[c]*Centre of Computational and Integrative Science, SRM University – AP, Amaravati 522240, Andhra Pradesh, India*

Now, as the intrinsic activity of TM–N–C single-atom catalysts (SACs) for various reduction reactions, including the $CO_2$RR, $N_2$RR, $NO_3$RR, $NO_2$RR, and ORR, is associated with the electronic structure of both the TM centre and the N-doped carbon support, fundamental understanding of complex electronic behaviour is required in designing superior and cost-effective catalysts. But, screening a large group of catalysts for the multi-step electrocatalytic $CO_2$RR and $NO_2$RR fundamentally is quite a challenging task. The same thing applies for urea formation in the simultaneous reduction of $CO_2$ and $NO_2^-$ using SACs, because SACs with strong activity individually for both $CO_2 \rightarrow CO$ and $NO_2^- \rightarrow NH_3$ reductions demonstrate higher reactivity for urea formation from the co-reduction of $CO_2$ and $NO_2^-$.[26] In this case, single atom catalysts operate as tandem catalysts which can reduce simultaneously $CO_2$ and N-based molecules ($N_2$, $NO_2^-$ and $NO_3^-$) to urea *via* the Eley–Rideal mechanism even if it has a single transition metal as the active site.[8,27] For that, simple electronic descriptors such as the d-band centre,[28–30] d-band frontier,[31] width corrected d-band centre[32] *etc.*, can provide insight into the origin and help to identify the promising $CO_2$RR, $NO_2$RR and their simultaneous reduction (urea formation) catalysts. But, in the case of TM–N–C SACs, the TM d-orbital splits into sub-d orbitals, thus it is better to focus on each sub-d orbital's contribution towards reactivity to find the electronic descriptor which can predict the catalytic activity.[33,34] In addition to this, the mechanism of C–N coupling which is an inevitable process for the formation of urea in the simultaneous reduction of $CO_2$ and nitrate or nitrite ions, is unclear. Some studies claim that, the co-existence of activated CO-like precursors and ammonia like precursors ($NH_2$) at the catalyst's surface, formed by simultaneous reduction of $CO_2$ and $NO_2^-$, is the obligatory condition for C–N coupling.[8,24,27,35] But, there is no theoretical proof which can support this point. Several studies with various metal catalysts have been reported, where the urea was synthesized by simultaneous reduction of $CO_2$ and $NO_2^-$ at gas-diffusion electrodes under mild conditions.[24,36,37] Thus, identifying a suitable descriptor that captures the complex electronic behaviour of the catalysts and elucidating the C–N coupling mechanism is crucial for further enhancing the performance of TM–N–C SACs in urea production *via* the simultaneous reduction of $CO_2$ and $NO_2$.

In this DFT study, the hybridization of the $d_{xz}$, $d_{yz}$, and $d_{z^2}$ orbitals of 3d and 4d transition metals (TMs) with orbitals of the adsorbate during three different reduction reactions, $CO_2$RR, $NO_2$RR and their simultaneous reduction on TM–N–C single-atom catalysts (SACs), was found to play a key role in determining catalytic reactivity. The manuscript will discuss that, among these d-orbitals, the $d_{yz}$ orbital plays the most significant role in predicting catalytic activity, showing strong linear correlations for the $CO_2$RR, $NO_2$RR and their simultaneous reduction across all 77 SACs. In the case of simultaneous reduction to produce urea on TM–N–C SACs, taking C–N coupling as an unavoidable phenomenon towards urea formation, we have come up with two mechanisms. Furthermore, the Gibbs free energy of adsorbed $NH_2$ was identified as an effective energy descriptor for accurately predicting urea formation activity *via* the two proposed mechanisms in the simultaneous reduction process. Finally using molecular orbital theory, we interpreted why $d_{yz}$ occupancy is the descriptor to identify catalysts for urea production.

## Results and discussion

### Structural details and stability

Many studies have explored that single-atomic-layer nitrogen-doped carbon has enough potential for TMs to be anchored, which leads to the formation of single atom catalysts (SACs).[38–41] Hence, in this work, to investigate the effects of N-doped different carbon supports along with TMs on the urea activity of TM–N–C SACs, we have selected seven types of single atom catalysts: TM–Pc, TM–$N_4$, TM–$N_3$C, TM–$N_2C_2$, TM–$NC_3$, TM–$C_4$ and TCNQ.[42] For each and every type of SAC, 11 transition metals, abundant in the earth, Cr, Co, Cu, Fe, Mn, Ni, Ru, Sc, V, Zn and Pd, are taken into account (see SI Fig. 1–3).[43] To check the thermodynamic stability for each catalyst we have obtained formation energy calculations (formula details given in the SI). In SI Table 1, we could observe that the most of the catalysts exhibit negative formation energies (specifically TMs coordinated with four N-atoms) which points out that the systems, considered in this work, are all thermodynamically stable. In addition, we have performed AIMD simulations for all types of systems: TM–$N_4$, TM–$N_3$C, TM–$N_2C_2$, TM–$NC_3$, TM–$C_4$, TM–Pc and TCNQ with Fe as the TM to cover all SACs for their thermodynamic stability at 300 K with 10 000 fs, each time step has time of 2 fs.[44] In the case of AIMD simulations, all seven SACs, having Fe as the transition metal, display good stability in terms of total electronic energy (see the Fig. 1h–j). And for the investigations of electrochemical stability, we have performed dissolution potential calculations for all the SACs. The details of the formula and the analysis of electronic stability at different applied potentials are provided in SI Table 6. The positive values of dissolution potentials for the SACs (specifically TMs coordinated with four N-atoms) convey that most of the systems are electrochemically stable (see SI Table 1).

### Selection of CO catalysts in $CO_2$ reduction

In the simultaneous reduction of $CO_2$ and nitrogen-based molecules (such as $N_2$, $NO_2^-$, or $NO_3^-$) for urea synthesis, CO formed from $CO_2$ serves as a key intermediate that couples with nitrogen-derived species, unlike other $CO_2$ reduction products such as HCOOH, $CH_4$, or $C_2H_4$, which do not take part in this coupling reaction. Before discussing $CO_2$ reduction and the potential for CO formation across all 77 SACs, we examined the effects of side reactions (HER) that can hinder the main reaction. Therefore, suppression of the HER is crucial to obtain the CO (g) product over $H_2$ (g). As the formation of $CO_2H$ or the desorption of CO (g) from the catalyst surface is the potential-determining step in $CO_2$ reduction, these two intermediates can be used to evaluate the selectivity of the $CO_2$RR over the HER.[23] For the selectivity analysis, the nine best catalysts out of all 77 SACs, which are capable of suppressing the HER while forming CO (g), are highlighted in Fig. 2a and b. These include Ni–Pc, Zn–Pc, Ni–TCNQ, Pd–TCNQ, Cu–$N_4$, Ni–$N_4$, Zn–$N_4$, Ni–$N_2C_2$ and

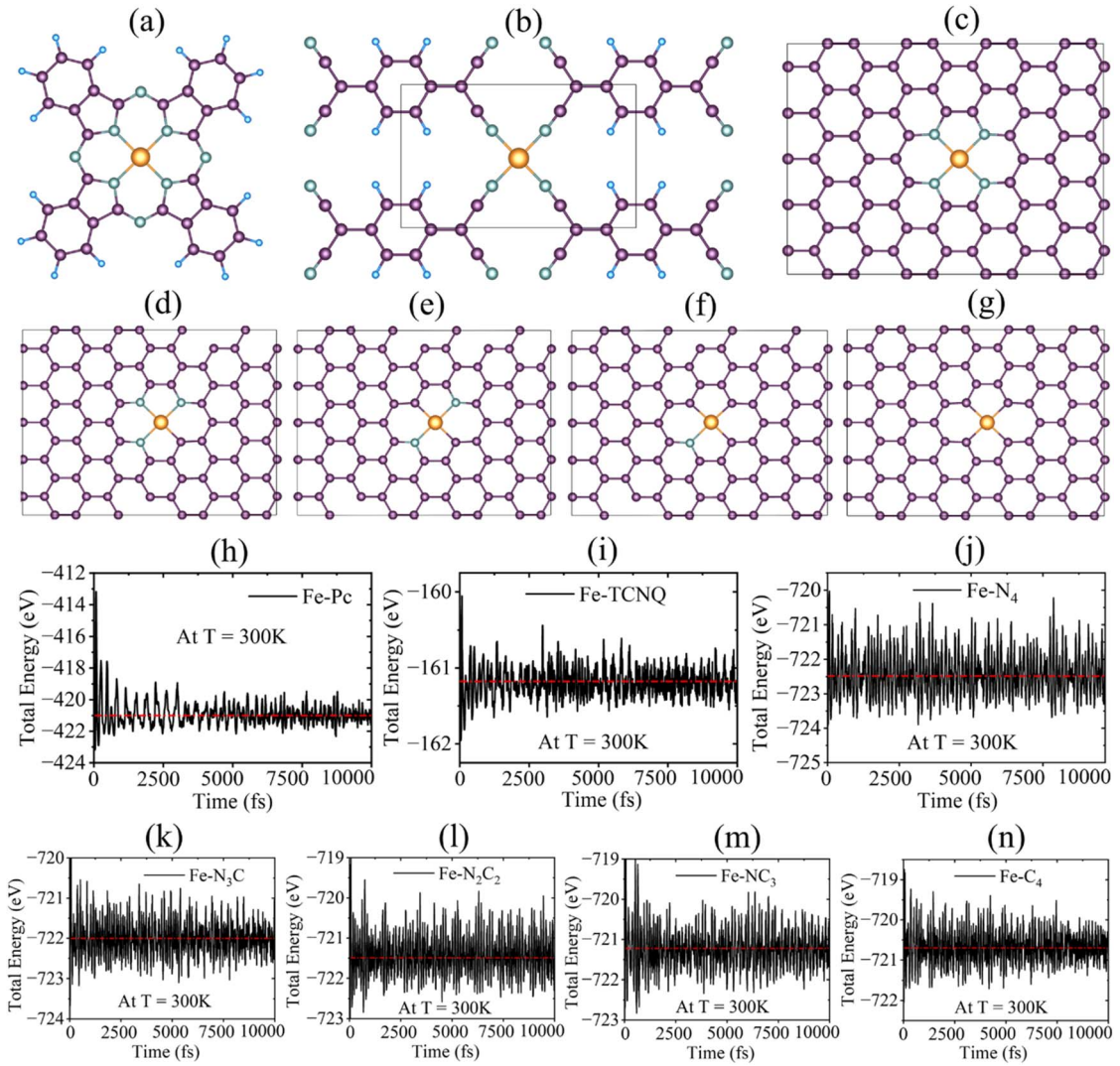


Fig. 1 (a)–(g) The optimized structures of Fe–Pc, Fe–TCNQ, Fe–$N_4$, Fe–$N_3C$, Fe–$N_2C_2$, Fe–$NC_3$ and Fe–$C_4$ respectively, and (h)–(n) the plots of total energy *vs.* time using *ab initio* molecular dynamics simulation for Fe–Pc, Fe–TCNQ, Fe–$N_4$, Fe–$N_3C$, Fe–$N_2C_2$, Fe–$NC_3$ and Fe–$C_4$ at $T$ = 300 K.

Zn–$N_2C_2$. The results for the remaining catalysts are provided in the SI. Fig. 2a shows that, relative to the reference level of 0.0 eV, all nine catalysts have higher hydrogen adsorption energy barriers than the highest thermodynamic barrier in the $CO_2 \rightarrow$ CO (g) pathway, which occurs at the first protonation step ($* + CO_2 + H^+ + e^- \rightarrow *CO_2H$). For instance, Ni–$N_2C_2$ exhibits a hydrogen adsorption barrier of 0.77 eV, while the first protonation step in the $CO_2 \rightarrow$ CO (g) pathway has a barrier of 0.71 eV, which is 0.06 eV lower than the hydrogen adsorption barrier. For Pd–TCNQ, Ni–TCNQ, Zn–$N_4$, Zn–$N_2C_2$, Ni–$N_4$, Cu–$N_4$, Ni–Pc and Zn–Pc, the values of the first protonation barrier, in the $CO_2 \rightarrow$ CO (g) pathway are 0.17, 0.07, 2.03, 0.02, 0.05, 0.18, 0.04 and 0.21 eV less than their corresponding hydrogen adsorption barriers, respectively. As shown in Fig. 2b, these nine catalysts favour the formation of CO (g) over CHO formation, which has a higher endothermic barrier. This preference is due to the lower energy required for CO desorption compared to CHO formation, with CHO formation barriers of 0.60, 0.80, 1.12, 1.17, 1.26, 1.38, 1.58, 1.71, and 1.99 eV for Ni–$N_2C_2$, Pd–TCNQ, Ni–TCNQ, Zn–$N_4$, Zn–$N_2C_2$, Ni–$N_4$, Cu–$N_4$, Ni–Pc, and Zn–Pc, respectively. The details of the $CO_2$RR mechanism, full free energy profile and comparison between the $CO_2$RR and HER for all other SACs are provided in SI Fig. 4–8 and Table 2.

In order to identify an electronic descriptor capable of predicting the free energy of the first protonation step ($\Delta G_{*CO_2H}$), which is the highest barrier in the $CO_2 \rightarrow$ CO (g) pathway and thus determines the activity, we conducted electronic structure analysis. Since $CO_2$ adsorbs in a horizontal configuration on the surface of single-atom catalysts, its molecular orbitals interact with the out of plane d-orbitals of the transition metal centre in the SAC. Therefore, the characteristics of these d-orbitals can be used to describe $CO_2$RR activity. Various combinations of these d-orbital contributions were tested to find correlations with the free energy of the first protonation step ($\Delta G_{*CO_2H}$) in the $CO_2 \rightarrow$ CO (g) pathway. Among all possible orbital combinations, occupancies of $d_{xz}$, $d_{z^2}$ and $d_{yz}$ exhibit a good linear correlation

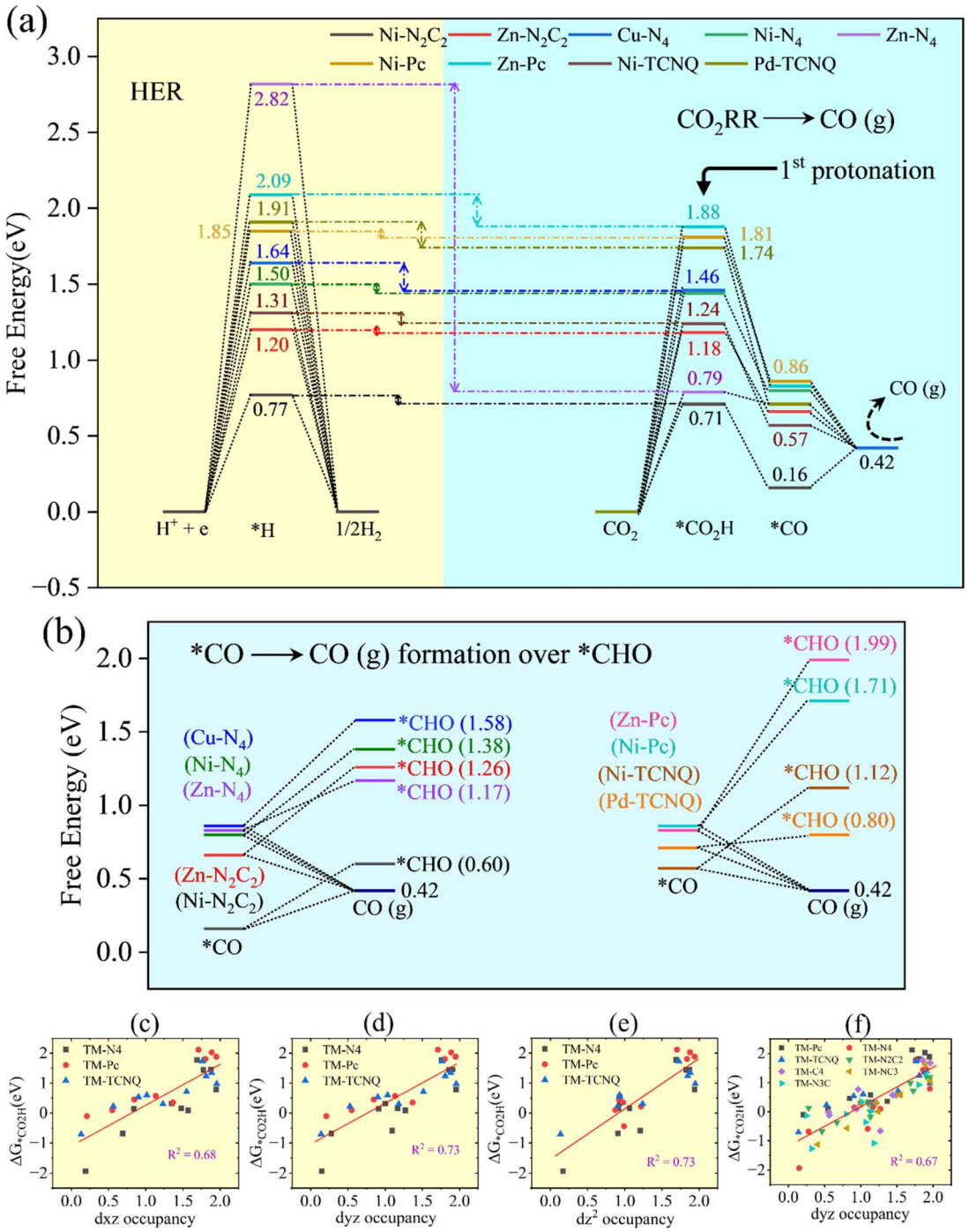


Fig. 2 (a) and (b) the comparison of $CO_2$RR and HER selectivity and CO (g) formation over CHO with the nine best SACs; (c)–(e) the correlation of occupancies of $d_{xz}$, $d_{yz}$ and $d_{z^2}$ orbitals with the free energy of the first protonation step in the $CO_2$ → CO (g) pathway for SACs with TMs coordinated with four N-atoms and (f) correlation of the occupancy of $d_{yz}$ with the free energy of the first protonation step in the $CO_2$ → CO (g) pathway with all 77 SACs.

with $\Delta G_{*CO_2H}$, with $R^2$ values of 0.68, 0.73 and 0.73, respectively, for SACs where the transition metal is coordinated by four nitrogen atoms (the most stable configurations), as shown in Fig. 2c–e.[34] When considering all 77 SACs, the $d_{yz}$ occupancy remains the most influential descriptor of reactivity, exhibiting an $R^2$ value of 0.67 (see Fig. 2f). For a particular sub d-orbital of TMs in SACs, the occupancy is calculated through integrating DOS up to the Fermi level ($-\infty$ to 0), the area under the curve as shown in SI Fig. S36.

### Selection of the $NH_3$ catalyst in reduction of $NO_2$ ions

Since nitrite ions exhibits a higher capability than nitrate ions for urea production during the simultaneous reduction of $CO_2$

and nitrogen-based molecules (such as $N_2$, $NO_2^-$, and $NO_3^-$), in this study, we focused on the nitrite reduction reaction mechanism for ammonia formation.[35–37] Similar to CO (g) formation during $CO_2$ reduction, the formation of $NH_3$ in nitrite reduction is also a necessary prerequisite for C–N coupling in the simultaneous reduction of $CO_2$ and nitrite ions to produce urea. As the HER is a common side reaction in aqueous medium for any reduction reaction (*e.g.* $CO_2$RR, NRR, ORR, $NO_3$RR, $NO_2$RR, *etc.*), examining the $NO_2$RR selectivity against the HER is inevitable.[17,23,38,40,45,46] All 77 SACs exhibit higher $NO_2^-$ adsorption energies compared to hydrogen adsorption energies, as presented in SI Fig. 5 and Table 3. Consequently, the reaction selectivity shifts towards the nitrite reduction reaction for ammonia production rather than hydrogen evolution.

For the selectivity assessment, the 11 most promising catalysts among the 77 SACs, which effectively suppress the HER while facilitating $NH_3$ formation, are presented in Fig. 3a and b. Among these 11 promising SACs, Zn–TCNQ emerged as the

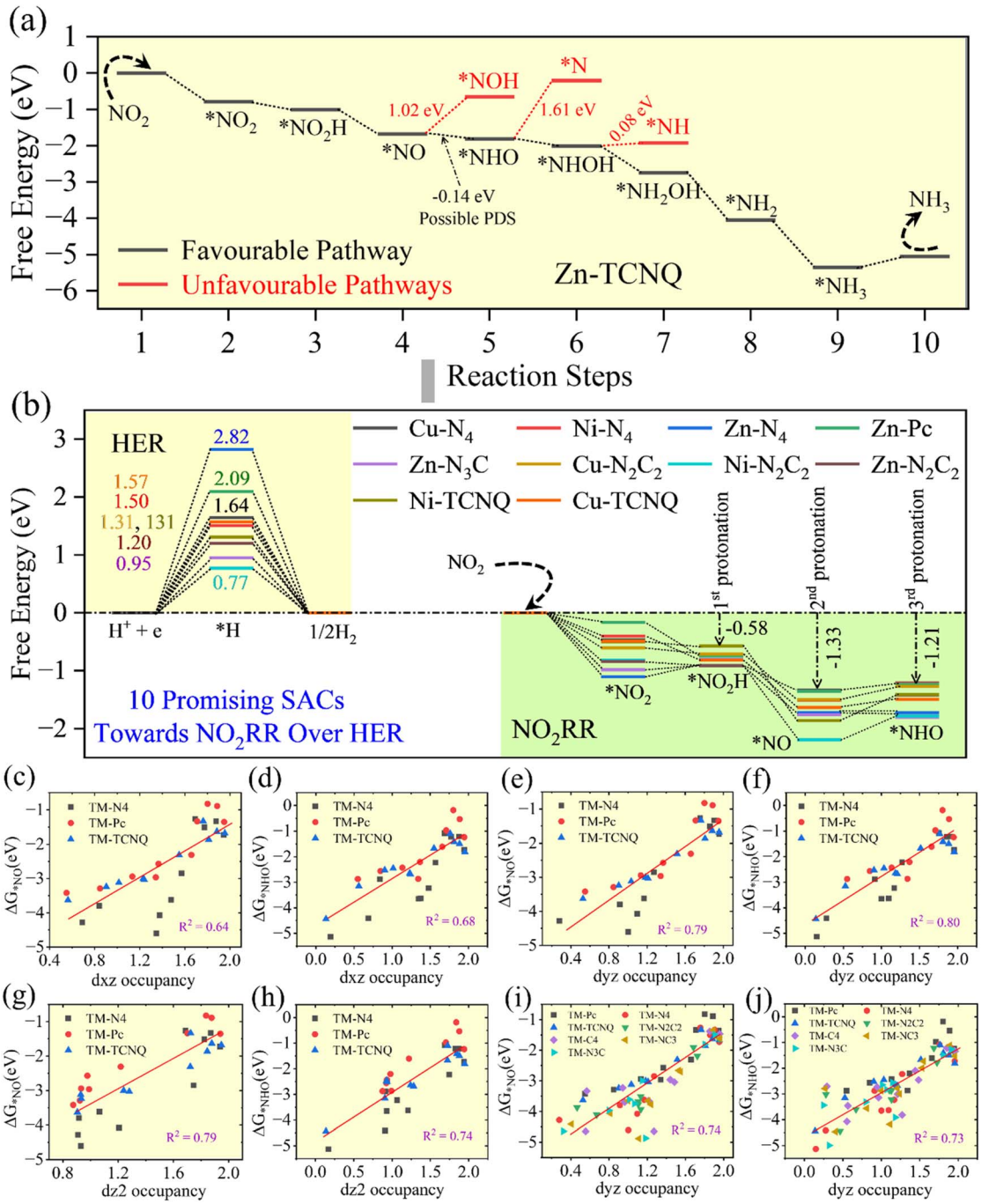


Fig. 3 (a) Full free energy profile of the $NO_2$RR on Zn-TCNQ, (b) the mechanisms of the HER *vs.* $NO_2$RR with the 10 best SACs, (c)–(h) the linear correlation of the adsorption free energy of NHO and NO with $d_{xz}$, $d_{yz}$ and $d_{z^2}$ occupancies for SACs with TMs coordinated with four N-atoms, and (i) and (j) correlation between occupancy of $d_{yz}$ and free energy of adsorbed NO and NHO for all 77 SACs.

most reactive catalyst, exhibiting a completely downhill free energy profile up to the *$NH_3$ intermediate, and having an HER barrier of 0.96 eV, as shown in Fig. 3a. Within this downhill profile, the *NO → *NHO step, which is slightly exothermic with a free energy change of −0.14 eV, can be considered the potential-determining step (PDS). Another 10 promising SACs have been showcased in Fig. 3b, having an endothermic reaction ($NO_2$RR) barrier (PDS), unlike Zn–TCNQ. For example, Ni–$N_2C_2$ shows HER limiting potential to be 0.77 eV, whereas in the $NO_2$RR it is 0.41 eV, noticed at step *NO → *NHO. For Zn–$N_3C$, Zn–$N_2C_2$, Ni–TCNQ, Cu–$N_2C_2$, Ni–$N_4$, Cu–TCNQ, Cu–$N_4$, Zn–Pc and Zn–$N_4$ the values of HER limiting potential are 0.95, 1.20, 1.31, 1.31, 1.50, 1.57, 1.64, 2.09 and 2.82 eV, and that of the $NO_2$RR are 0.18 (at *$NO_2$ → *$NO_2$H), 0.22 (at *NO → *NHO), 0.45 (at *NO → *NHO), 0.23 (at *NO → *NHO), 0.29 (at *NO → *NHO), 0.14 (at *NO → *NHO), 0.12 (at *NO → *NHO), 0.12 (at *NO → *NHO) and 0.30 eV (at *$NO_2$ → *$NO_2$H), respectively. The detailed $NO_2$RR mechanism, full free energy profile and comparison with HER activity and PDS values of other SACs are provided explicitly in SI Fig. 5, 9–11 and SI Table 3.

In the case of $NO_2^-$ reduction, configuration of adsorbed nitrite molecules follows an end-on fashion, where N of $NO_2$ exists on top of the TM of the SAC, as shown in SI Fig. 5. And the activation of the $NO_2$ molecule can be considered as follows: the hybridized $sp^2$ orbital of N@$NO_2$ couples with the out of plane d-orbitals ($d_{xz}$, $d_{yz}$ and $d_{z^2}$) of the TM atom. Hence, these d-orbitals might be helpful in demonstrating the $NO_2$RR activity. Several combinations of these d-orbitals were examined to have a linear correlation with the limiting potential of the catalysts, but nothing worked out. Instead, we have obtained a good linear correlation between the free energy of the two intermediates (*NO and *NHO) and occupancies of $d_{xz}$, $d_{yz}$ and $d_{z^2}$ orbitals of TMs, shown in Fig. 3c–h (considering SACs with TMs coordinated with four nitrogen atoms, showing higher structural stability). Out of these sub-d orbitals, occupancy of $d_{yz}$ played a significant role in predicting reactivity of the catalysts, having $R^2$ values of 0.79 and 0.80 for *NO and *NHO, respectively.[34] Furthermore, we tested occupancy of $d_{yz}$ for all 77 SACs and found $R^2$ to be 0.74 and 0.73, which is a good correlation for predicting reactivity (see Fig. 3i and j). Once these two free energies are predicted, we can predict the catalytic activity of a random SAC catalyst, as most of the SACs displayed step *NO → *NHO as the PDS.

We also examined the linear correlation between the $d_{yz}$ occupancy and $\Delta G_{*CO_2H}$, $\Delta G_{*NO}$ and $\Delta G_{*NHO}$ after including the Ti–Pc SAC, considering Ti as the transition metal (from the 3d block), and observed no significant change in the $R^2$ values (see SI Fig. 35). Therefore, it can be inferred that the $R^2$ value would remain nearly unchanged upon including Ti as the transition metal for the other six types of differently coordinated TM–N–C SACs.

### Simultaneous reduction of $CO_2$ and nitrite ions ($NO_2^-$)

In the above sections, we have elucidated the individual performance of the 77 SACs in cases of $CO_2$ and nitrite ions reduction reactions. We observed that a greater number of SACs prefer CO (g) as well as $NH_3$ formation during $CO_2$ and $NO_2^-$ reduction, respectively. For simultaneous reduction of $CO_2$ and nitrite ions towards urea formation, C–N coupling is a crucial step. Thus, in the simultaneous reduction reaction, which can form CO (g) and $NH_3$ as well, the generated CO (g) molecule can either couple with N-based intermediates ($NO_2$, $NO_2H$, N, and NH, $NH_2$) or with the $NH_2^-$ (amino) radical, leading to the formation of the C–N bond. The N-based intermediates are generated *via* $NO_2^-$ → $NH_3$ (nitrite ions to ammonia), whereas $NH_2^-$ (amino) radicals are generated through interaction of the $OH^-$ radical with ammonia ($NH_3 + OH^- \rightarrow NH_2^-$). But, single atom catalysts, having the metal centre as the only active site, behave as a tandem catalyst towards C–N bond formation *i.e.*, they follow the Eley–Rideal mechanism for the formation of the C–N bond. Now, because of so many N-based intermediates formed during nitrite ion reduction, finding a suitable N-based intermediate as a precursor for C–N bond formation is an important task. In the case of intermediates *$NO_2$, *$NO_2$H and *N, the nitrogen (N)-atom has less charge, because highly electronegative oxygen atoms are connected to nitrogen (N) (for *$NO_2$ and *$NO_2$H), and the TM is connected to N (for *N). Thus, C–N coupling through CO and these intermediates cannot be taken into account. On the other hand, the N-atom in NH and $NH_2$, activated on the catalyst surface, has enough charge, accepted from the bonded hydrogen atom, to couple with CO, forming the C–N bond. But, C–N coupling through CO and NH molecules is very strong, in terms of free energy, which leads to a higher thermodynamic barrier towards urea formation compared to the case of CO and $NH_2$ coupling (moderate in terms of free energy), as depicted in Fig. 4b and c. Quantitatively, we also confirmed with Bader charge analysis, where we have seen that the charge on N in *$NH_2$ is comparatively greater than the any other N-based intermediate including *NH, *$NO_2$, *$NO_2$H, and *N, as provided in the Fig. 4a. The C–N coupling through CO (pre) and $NH_2$ (pre) is also agreed by Shibata *et al.* reported in 2003.[24] In their study, TM–Pc SACs: Co–Pc, Cu–Pc, Ni–Pc, Fe–Pc, Mn–Pc, Pd–Pc and Zn–Pc displayed promising catalytic activity in the simultaneous reduction of $CO_2$ and $NO_2^-$ towards urea formation. On the contrary, Cr–Pc, Mo–Pc, Ru–Pc, Sc–Pc and V–Pc were found to be poor catalysts towards urea formation. If C–N coupling occurs through CO and NH, the poor catalysts for urea formation show, in our DFT simulations, moderate C–N coupling in terms of free energy, whereas for promising catalysts opposite phenomena can be observed, *i.e.*, strong C–N coupling, leading to a greater reaction barrier. This observation is contradictory to the experimental work for urea formation in the simultaneous reduction of $CO_2$ and $NO_2^-$.[24] Therefore, as a nitrogen-based molecule either the amino radical ($NH_2^-$) or activated $NH_2$ intermediate functions as a precursor for C–N coupling in the direction of urea formation.

### Activation of CO and $NH_2$ for C–N coupling

Activation of the two precursors CO (pre) and $NH_2$ (pre), generated through simultaneous reduction of $CO_2$ and nitrite ions, can be demonstrated by adsorption or binding energy. The value of binding energy for $NH_2$ (pre) is greater than that of CO

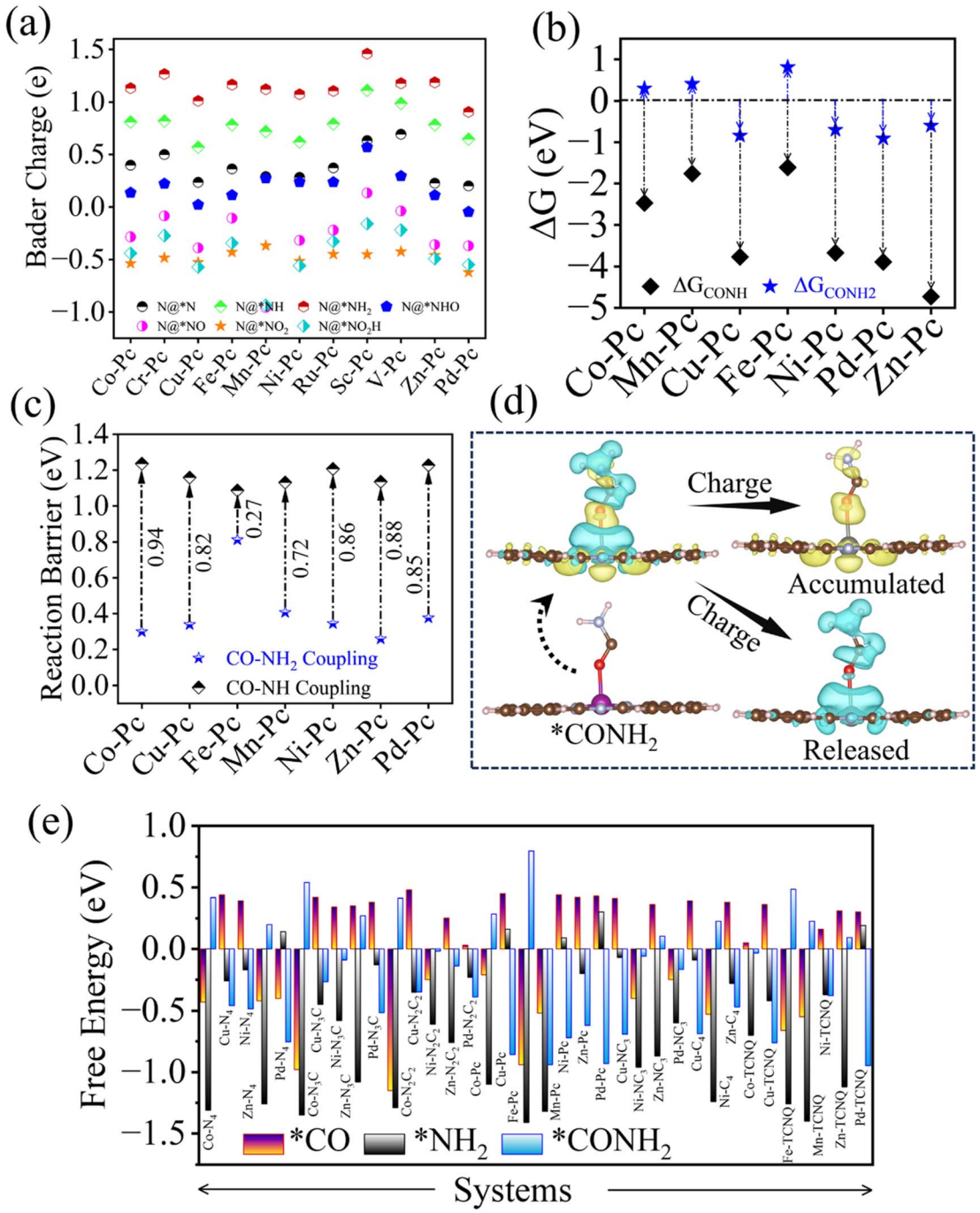


Fig. 4 (a) The Bader charge of the N-atom in the intermediates *N, *NH, *$NH_2$, *NO, *NHO, *$NO_2$ and *$NO_2H$ of all TM–Pc SACs, (b) comparison of Gibbs free energy during CO–NH and CO–$NH_2$ coupling, (c) the reaction barrier during urea formation for two possible coupling CO–NH and CO–$NH_2$ pathways and (d) the charge density difference during CO–$NH_2$ coupling for TM–Pc SACs. (e) Comparison of adsorption energy of *CO, *$NH_2$ and *$CONH_2$.

(pre) for all 77 SACs, which means that $NH_2$ (pre) will occupy the metal centre over CO (pre). This can be concluded from the PDOS plots of adsorbed CO and $NH_2$, where the density of states for $NH_2$ (pre) observed to be spread over the energy range compared to the case of CO (pre) (see SI Fig. 15–19). In addition, Bader charge analysis of adsorbed $NH_2$ (pre) and CO (pre) reveals that the $NH_2$ adsorption, having a greater charge on it, is favoured over CO on the metal site (see SI Table 5). Since SACs have a single metal centre as their active site for any reaction to happen, co-existence of CO (pre) and $NH_2$ (pre) can be expected for the C–N coupling *via* the Eley–Rideal mechanism. And the co-existence of precursors can only be possible if the adsorption or desorption free energy for both the precursors is moderate, not more negative than −1.5 eV.

Based on the values of the adsorption energy or desorption barrier of $NH_2$ (g) and CO (g) in the range of −1.5 to 1.5 eV, we have selected 36 SACs among the 77 SACs, see Fig. 4e. Two mechanisms of urea formation are proposed in the simultaneous reduction of $CO_2$ and nitrite ions which can be described as follows:

Mechanism-01:

$$CO + NH_2 + * \rightarrow CO + *NH_2 \quad (1)$$

$$CO + *NH_2 \rightarrow *CONH_2 \quad (2)$$

$$*CONH_2 + NH_2 \rightarrow *CO(NH_2)_2 \quad (3)$$

Mechanism-02:

$$CO + NH_2 + * \rightarrow CO + *NH_2 \quad (4)$$

$$CO + *NH_2 \rightarrow *CONH_2 \quad (5)$$

$$*CONH_2 + NO_2 \rightarrow *NO_2CONH_2 \quad (6)$$

$$*NO_2CONH_2 + H^+ + e \rightarrow *NO_2HCONH_2 \quad (7)$$

$$*NO_2HCONH_2 + H^+ + e \rightarrow *NOCONH_2 + H_2O \quad (8)$$

$$*NOCONH_2 + H^+ + e \rightarrow *NOHCONH_2 + H_2O \quad (9)$$

$$*NOHCONH_2 + H^+ + e \rightarrow *NCONH_2 + 2H_2O \quad (10)$$

$$*NCONH_2 + H^+ + e \rightarrow *NHCONH_2 + 2H_2O \quad (11)$$

$$*NHCONH_2 + H^+ + e \rightarrow *CO(NH_2)_2 + 2H_2O \quad (12)$$

In the 1st mechanism, first, $NH_2$ approaches the active site of a given catalyst and gets adsorbed on it. Next, it couples with CO in the 2nd step to form the C–N bond which transforms into $CONH_2$. Lastly, another $NH_2$ (pre) approaches towards adsorbed $CONH_2$ and interacts with it, resulting in the formation of urea ($CO(NH_2)_2$). Whereas in the 2nd mechanism, upon activation of $CONH_2$, formed through coupling of CO and $NH_2$, one nitrite ion ($NO_2^-$) approaches the C of adsorbed intermediate $*CONH_2$, forming $*NO_2CONH_2$. Next, hydrogenation takes place one by one until $CO(NH_2)_2$ is formed and finally desorbs from the catalyst.

The reaction steps 1 and 2 of the 1st mechanism resemble the steps 1 and 2 of the 2nd mechanism, and the last step of each mechanism yields urea ($CO(NH_2)_2$) as the final product. Hence, taking the 2nd mechanism into account, in making the free energy profile towards urea formation, is enough to examine each and every intermediate state whether it is endothermic or exothermic. In the case of TM–Pc SACs, we observed that TMs such as Co, Cu, Ni, Fe, Mn, Zn, and Pd have the ability of producing urea with limiting potential values of 0.28, 0.34, 0.34, 0.8, 0.41, 0.26 and 0.38 V, respectively. On the other hand, other four (Cr–Pc, Ru–Pc, Sc–Pc and V–Pc) are neglected due to the higher binding of $NH_2$ (<−1.5 eV) to the TM centre, poisoning the catalyst. The PDS values of the reaction mechanism for all these seven catalysts are observed to be either at $*NH_2 + CO \rightarrow *CONH_2$ or $*CONH_2NO_2 \rightarrow *CONH_2NO_2H$. For Co–Pc, Fe–Pc and Mn–Pc it is at $*NH_2 + CO \rightarrow *CONH_2$ and others follow the 2nd one. This agrees with the results reported by Shibata *et al.* where they demonstrated that the TM–Pc SACs with TMs such as Cr, Mo, Ru, Sc and V were unable to form urea, whereas TM–Pc SACs with Co, Ni, Cu, Fe, Zn, Pd and Cd displayed a better picture in the direction of urea formation.

The same concept was applied for the other SACs ($TM–N_4$, $TM–N_3C$. $TM–N_2C_2$, $TM–NC_3$, $TM–C_4$ and TCNQ), in the simultaneous reduction of $CO_2$ and nitrite ions towards urea formation. Most of the catalysts in these other types of SACs, which are able to form urea like TM–Pc SACs, display PDS at $*CONH_2NO_2 \rightarrow *CONH_2NO_2H$ and some at step $*NH_2 + CO \rightarrow *CONH_2$. The detailed explanation of each and every type of SACs, with the full free energy profile, is provided in SI Fig. 12–14. All the PDS values either at $*NH_2 + CO \rightarrow *CONH_2$ or $*CONH_2NO_2 \rightarrow *CONH_2NO_2H$ are presented in Fig. 5b, denoted as PDS1 ($\eta_1$) and PDS2 ($\eta_2$), respectively.

Among the 36 SACs, which are able to form urea, 13 SACs show an endothermic barrier at $*NH_2 + CO \rightarrow *CONH_2$ *i.e.*, during C–N coupling. The remaining 23 SACs display a spontaneous process of C–N bond formation. In addition, we have performed climbed nudged elastic band (NEB) calculations to investigate the kinetic barrier of C–N coupling between $NH_2$ (pre) and CO (pre), where, $NH_2$ is considered to be adsorbed on the metal centre and that of CO is on the C-atom near to the metal centre. Catalysts, having an endothermic barrier in the formation of the C–N bond, exhibit a greater kinetic barrier compared to the case of exothermic formation of the C–N bond as shown in SI Fig. 33. Therefore, catalysts displaying spontaneous formation of the C–N bond are considered to be promising catalysts for urea formation in the simultaneous reduction of $CO_2$ and $NO_2^-$. Among 23 SACs, ten are found to be the best catalysts for the reaction: Cu–Pc, Ni–Pc, Zn–Pc, Pd–Pc, Cu–TCNQ, Ni–TCNQ, Pd–TCNQ, $Cu–N_4$, $Ni–N_4$ and $Pd–N_4$.

### Correlation of the energy descriptor with limiting potential

In the case of mechanism-01, the coupling intermediate (step 2 $*NH_2 + CO \rightarrow *CONH_2$) is the main potential determining step to decide how much external energy needs to be supplied to the system for the reaction to occur. Thus, a linear type of correlation with this coupling free energy, PDS1 ($\eta_1$), with an electronic or any intermediate energy parameter can be a great finding. Here, we have tried with CO and $NH_2$ binding energy to get a linear correlation with this coupling free energy. The adsorption free energy of $NH_2$, $\Delta G_{*NH_2}$, shows a good linear correlation with this coupling free energy, PDS1 ($\eta_1$), with $R^2 = 0.93$ as depicted in Fig. 5d. In addition, we also tried, considering TM–Pc SACs, to correlate the transition state barrier with $\Delta G_{*NH_2}$. And we observed a very good correlation between them, having $R^2 = 0.99$. Then, considering plots of Fig. 5d and e, we explored all SACs, which are able to form urea, through a BEP relation with $R^2 = 0.99$ (see Fig. 5f). Thus, the $NH_2$ adsorption binding energy functions as an energy descriptor to find the catalytic activity towards urea formation in the simultaneous reduction of $CO_2$ and $NO_2^-$.

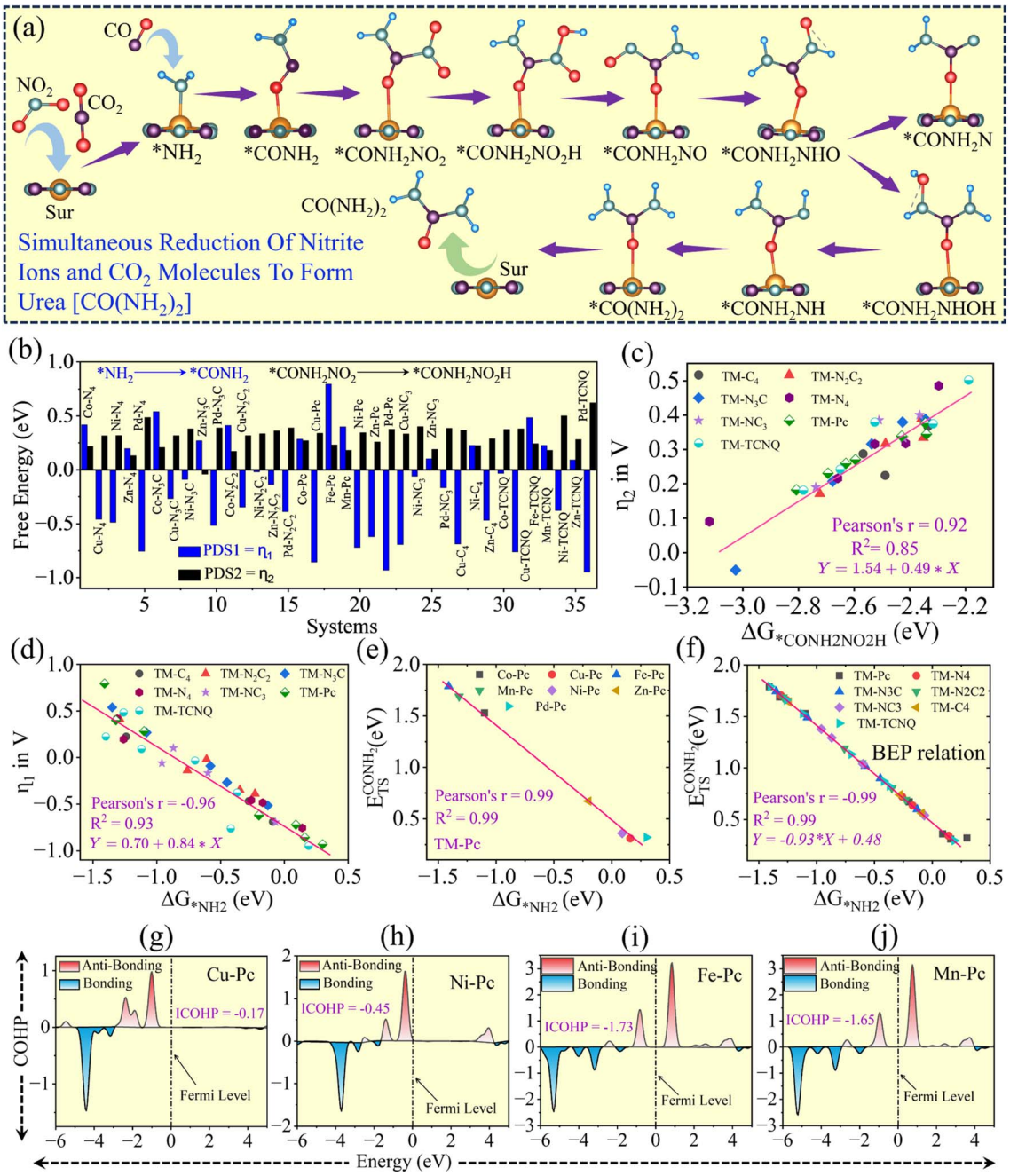


Fig. 5 (a) The schematic of the full free energy of urea formation, (b) PDS1 and PDS2 of all SACs able to form urea, (c) correlation of PDS2 with the adsorption free energy of $CONH_2NO_2H$, (d) the correlation of PDS1 with the adsorption free energy of $NH_2$, (e) the correlation of the transition state energy of $*CONH_2$ with the adsorption free energy of $NH_2$, (f) the BEP relation of transition state energy of $*CONH_2$ with adsorption free energy of $NH_2$, and (g) to (j) COHP of Cu–Pc, Ni–Pc, Fe–Pc and Mn–Pc.

In the case of mechanism-02, the potential determining step can be observed either at $*NH_2 + CO \rightarrow *CONH_2$ or $*CONH_2NO_2 \rightarrow *CONH_2NO_2H$. Thus, either PDS1 ($\eta_1$) or PDS2 ($\eta_2$) would be the PDS for the mechanism-02. If PDS1 ($\eta_1$) > PDS2 ($\eta_2$), adsorption energy of $NH_2$ can be used as an energy descriptor for finding catalytic activity, otherwise we need a new energy parameter for the same. We investigated correlations of the adsorption free energy $\Delta G_{*CONH_2NO_2}$ and $\Delta G_{*CONH_2NO_2H}$ with the limiting potential ($\eta_2$). The linear correlation between $\Delta G_{*CONH_2NO_2}$ and the limiting potential ($\eta_2$) is not up to the mark, whereas in between $\Delta G_{*CONH2NO_2H}$ and the limiting potential ($\eta_2$) it unveils an interesting result. The linear correlation of $\Delta G_{*CONH_2NO_2H}$ with $\eta_2$ is $R^2 = 0.86$ (neglecting 4 SACs, three from 3d block: Zn–$N_4$, Zn–$N_2C_2$, Zn–TCNQ and one from 4d block: Pd–TCNQ) (see Fig. 5c). So, $\Delta G_{*CONH_2NO_2}$ acts as an energy descriptor to predict catalytic activity in terms of limiting potential in the 2nd mechanism of urea formation from simultaneous reduction of $CO_2$ and $NO_2^-$ (if PDS1 ($\eta_1$) < PDS2 ($\eta_2$)).

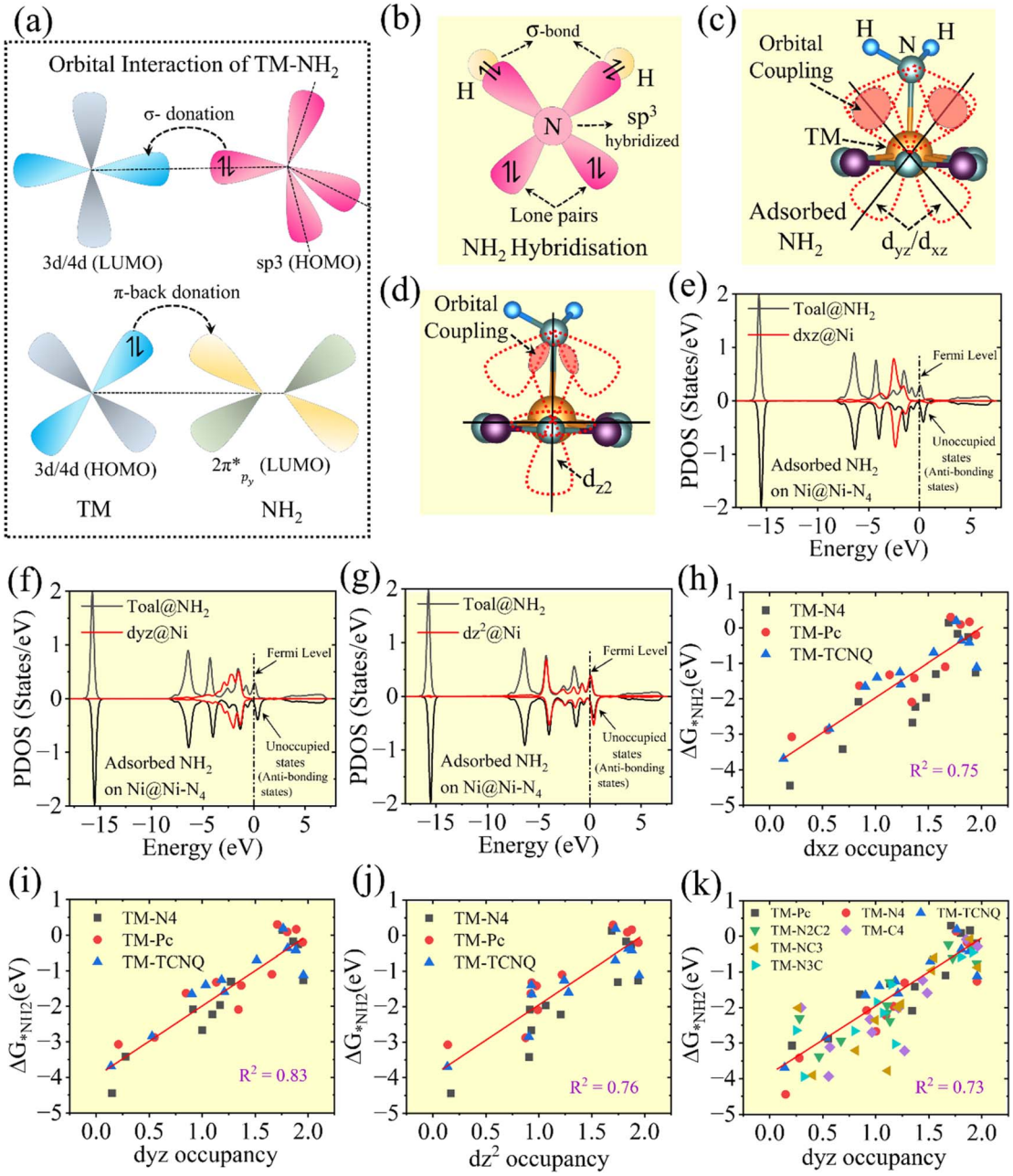


Fig. 6 (a) The orbital interaction between adsorbed $NH_2$ with the TM of the SAC, (b) schematic of hybridization of the free $NH_2$ molecule, (c) and (d) schematic of coupling of the $sp^3$ hybridized orbitals of $NH_2$ with $d_{xz}$, $d_{yz}$ and $d_{z^2}$ orbitals of the TM of the SAC, (e)–(g) the PDS of adsorbed $NH_2$ and the sub-d orbital of the TM of the SAC showing coupling between total DOS of adsorbed $NH_2$ with $d_{xz}$, $d_{yz}$ and $d_{z^2}$ orbitals of the TM, (h)–(j) correlation of occupancies of $d_{xz}$, $d_{yz}$ and $d_{z^2}$ with free energy of adsorbed $NH_2$ for SACs with TMs coordinated with four N-atoms and (k) correlation between occupancy of $d_{yz}$ and free energy of adsorbed $NH_2$ for all SACs.

To see the effects of the electric field and water solvent on the adsorption energies of the reaction intermediates and reaction barriers, we performed two types of DFT calculations: one including an external electric field and the other incorporating the effect of a water solvent. For the electric field calculations, a strong field of $-0.52 \times 10^{10}$ V $m^{-1}$ was applied, and the adsorption energies were computed for all three types of reactions considered in this work on TM–Pc SACs containing nine transition metals (TM = Co, Cr, Cu, Fe, Mn, Ni, Ru, Sc, and V). Similarly, implicit DFT solvent calculations were performed on the same systems. In both the cases, a constant shift of adsorption energies can be observed (see SI Fig. 37 and 38), which signifies that the overall trend of the reactivity across all the systems remains constant. The explicit values of adsorption energies, required to find reactivity of a catalyst, and the reaction barrier of the nine TM–Pc SACs for the three different reactions have been provided in SI Table 7–12. So, our work performed with DFT using the CHE model remains reliable.

To validate the DFT calculations using the GGA PBE functional, we have used another functional which is the revised

GGA PBE. The obtained values of free energies of all possible intermediates required for finding the PDS in the case of all TM–Pc SACs, done with the RPBE functional, are provided in SI Table 4. We observed that the difference of limiting potential for a particular TM–Pc SAC with two different functionals GGA PBE and GGA RPBE is very small. So, our simulated values are validated.

### Origin of catalytic activity towards urea formation

To explore the activation of $NH_2$ (axial ligand) on the TM in SACs, we presented a molecular orbital diagram in Fig. 6a. Here, we have shown that the $sp^3$ hybrid orbital of $NH_2$ (HOMO) is donating an electron (σ-donation) to the unoccupied d-orbital of the TM (LUMO), while the occupied d-orbital of the TM (HOMO) is donating an electron (π*-donation) back to the unoccupied antibonding orbital of $sp^3$ of $NH_2$. The pronounced σ donation and π* back-donation during $NH_2$ adsorption at the TM sites are responsible for its enhanced activation as first reported by the Blyholder model for CO activation.[47] Furthermore, we evaluated the $NH_2$ binding strength through three different analyses. Firstly, we investigated the position of the frontier orbitals (FOs) of the transition metal (TM) centres in the single-atom catalysts (SACs). These FOs, electronic states located near to the Fermi level, play a crucial role in governing the interaction between the TM site and the adsorbate. When the energy gap between the TM's FOs and the HOMO or LUMO of the $NH_2$ molecule is small, a reasonable orbital overlap and charge transfer occur, leading to stronger binding. Conversely, when the FOs of the TM are located farther from the Fermi level, the orbital interaction with $NH_2$ becomes less efficient, resulting in weaker adsorption strength (see the SI Fig. 21, 23 and 25).[48] Secondly, we examined the contribution of individual d-sub orbitals to the coupling: in the case of coupling between TM–N–C SACs and $NH_2$, the out of plane orbitals ($d_{xz}$, $d_{yz}$, and $d_{z^2}$) are responsible for TM–$NH_2$ bond formation (see Fig. 6b–g from the orbital and partial density of states point of view). The more the orbitals are coupled, the stronger the bond becomes. Thirdly, we performed crystal orbital Hamiltonian population (COHP) analysis: in order to identify the bonding and antibonding states below the Fermi level, COHP of the $NH_2$ bond with TM–N–C SACs is performed.[49–51] If the occupied bonding states are greater than the occupied anti-bonding states, the bond is considered to be enough strong to bind $NH_2$ or *vice versa* (see Fig. 5g–j and SI Fig. 27). By taking these three electronic points into account, we have examined thirty possible electronic features to correlate with the free energy of adsorbed $NH_2$, $\Delta G_{*NH_2}$ (see SI Fig. 28–32), thus determining the urea activity. Among the 30 performed possible electronic features (namely d-band centre, d-band occupancy, $d_{xz}$, $d_{yz}$ and $d_{z^2}$ centres and occupancy-based features with spin up and spin down components), occupancies of $d_{xz}$, $d_{yz}$ and $d_{z^2}$ orbitals exhibit a very good linear correlation with $\Delta G_{*NH_2}$ as presented in Fig. 6h–j having an $R^2$ value of 0.75, 0.83 and 0.76, respectively (presented for SACs with TMs coordinated with four nitrogen atoms).[34] As occupancy of $d_{yz}$ plays an important role in predicting urea reactivity of catalysts, we tested on all 77 SACs and found $R^2$ to be 0.73 (see Fig. 6k). Therefore, occupancy of $d_{yz}$ behaves as an electronic descriptor to accurately predict the urea activity on TM–N–C SACs. Overall, we can infer that the catalysts, having moderate orbital coupling and greater occupied anti-bonding states which lead to the moderate binding of $NH_2$ with TMs, will show superior activity in the simultaneous reduction of $CO_2$ and $NO_2^-$ towards urea formation such as Cu-Pc, Cu–$N_4$, Cu–TCNQ, Ni–Pc, Ni–$N_4$, Ni–TCNQ, Zn–$N_4$, Zn–Pc, Zn–TCNQ, Pd–Pc, Pd–$N_4$ and Pd–TCNQ. For further validation, linear regression with cross-validation was carried out, and the corresponding MAE (Mean Absolute Error) and RMSE (Root Mean Squared Error) values along with the 95% confidence band are presented in SI Fig. 39.

## Conclusion

In summary, we have successfully performed DFT simulations for the screening of (i) CO catalysts during $CO_2$ reduction, (ii) ammonia catalysts from nitrite ions reduction and (iii) urea catalysts in the simultaneous reduction of $CO_2$ and nitrite ions, respectively. In the case of $CO_2$ reduction, the number of CO (g) promising catalysts is found to be nine from all types of SACs which can suppress the HER and CHO formation as well. For the $NO_2$RR, the number of best ammonia catalysts is eleven which can suppress the HER among all types of SACs (total 77). In the case of urea formation in the simultaneous reduction, we proposed two mechanisms and illustrated the C–N coupling mechanism comparing the reaction energy barrier and using Bader charge analysis. And we found out that only the intermediate $NH_2$ can couple with CO for the given reaction. In further studies, we obtained $NH_2$ adsorption free energy as the energy descriptor to accurately find the catalytic activity towards urea formation which has a good linear correlation with limiting potential ($R^2 = 0.93$) and transition state energy of intermediate $CONH_2$ ($R^2 = 0.99$). Another energy descriptor $\Delta G_{*CONH_2NO_2H}$ was identified for the simultaneous reduction of $CO_2$ and nitrite ions which also has a good correlation with the catalytic activity in terms of limiting potential ($R^2 = 0.86$). From the electronic point of view, d-sub orbitals especially out of plane orbitals are observed to be the origin of urea activity. The occupancy of $d_{yz}$ shows a very good linear correlation with the adsorption free energy of $NH_2$, with an $R^2$ value of 0.83 for SACs where the transition metal is coordinated by four nitrogen atoms, and 0.73 when considering all 77 SACs. Overall, this descriptor-based theoretical study encourages, in the field of materials science, designing efficient SACs for urea formation in the simultaneous reduction of $CO_2$ and nitrite ions, and further motivates exploration of different groups of catalysts (metal, metal-based alloy, metal oxide *etc.*) for urea formation by the simultaneous reduction of $CO_2$ and N-based molecules ($N_2$, $NO_2^-$ and $NO_3^-$).

## Author contributions

Narad Barman: contributed to conceptualization, data curation, investigation, methodology (done all the calculations), formal analysis, data visualization, writing original draft, and

manuscript review and editing. Chiranjib Majumder: formal analysis, validation, and review and editing of the manuscript. Ranjit Thapa: conceptualized and designed the project, supervised the project, data curation, validation, writing the original draft, manuscript review and editing, and funding acquisition.

## Conflicts of interest

The authors declare no conflict of interest.

## Data availability

The data supporting this article have been included as part of the supplementary information (SI). Supplementary information is available. See DOI: https://doi.org/10.1039/d5sc06657c.

## Acknowledgements

NB thanks the University Grants Commission (UGC) for supporting the Fellowship under NFSC (No. F. 82-44/2020 (SA-III)). RT thanks the Board of Research in Nuclear Sciences (BRNS), India, for the financial support (Grant No. 58/14/13/2023-BRNS) and the Anusandhan National Research Foundation (ANRF), India (Grant No. CRG/2021/000620). The authors thank the SRM University-AP, Andhra Pradesh, for providing the central computational facility and National Supercomputing Mission (NSM) for providing access to PARAM Rudra for conducting DFT based computation. Thanks to Mr Sourav Ghosh for helping in estimation of MAE/RMSE.

## References

1 J. Liu, S. C. Smith, Y. Gu and L. Kou, C–N Coupling Enabled by N–N Bond Breaking for Electrochemical Urea Production, *Adv. Funct. Mater.*, 2023, **33**(47), 2305894, DOI: 10.1002/adfm.202305894.

2 X. Zhang, E. A. Davidson, D. L. Mauzerall, T. D. Searchinger, P. Dumas and Y. Shen, Managing Nitrogen for Sustainable Development, *Nature*, 2015, 51–59, DOI: 10.1038/nature15743.

3 C. Smith, A. K. Hill and L. Torrente-Murciano, Current and Future Role of Haber-Bosch Ammonia in a Carbon-Free Energy Landscape, *Energy Environ. Sci.*, 2020, **13**(2), 331–344, DOI: 10.1039/c9ee02873k.

4 X. Wei, Y. Liu, X. Zhu, S. Bo, L. Xiao, C. Chen, T. T. T. Nga, Y. He, M. Qiu, C. Xie, D. Wang, Q. Liu, F. Dong, C. L. Dong, X. Z. Fu and S. Wang, Dynamic Reconstitution Between Copper Single Atoms and Clusters for Electrocatalytic Urea Synthesis, *Adv. Mater.*, 2023, **35**(18), 2300020, DOI: 10.1002/adma.202300020.

5 M. Sun, G. Wu, J. Jiang, Y. Yang, A. Du, L. Dai, X. Mao and Q. Qin, Carbon-Anchored Molybdenum Oxide Nanoclusters as Efficient Catalysts for the Electrosynthesis of Ammonia and Urea, *Angew. Chem., Int. Ed.*, 2023, **62**(19), e202301957, DOI: 10.1002/anie.202301957.

6 J. Shao, N. Meng, Y. Wang, B. Zhang, K. Yang, C. Liu, Y. Yu and B. Zhang, Scalable Electrosynthesis of Formamide through C–N Coupling at the Industrially Relevant Current Density of 120 MA $Cm^{-2}$, *Angew. Chem., Int. Ed.*, 2022, **61**(44), e202213009, DOI: 10.1002/anie.202213009.

7 X. Zhu, X. Yuan, Y. Wang, M. Ge and Y. Tang, Advancing Electrocatalytic Urea Synthesis: Insights from 2D Benzenehexathiolate Coordination Nanosheets, *J. Catal.*, 2024, **429**, 115218, DOI: 10.1016/j.jcat.2023.115218.

8 Y. Gao, J. Wang, M. Sun, Y. Jing, L. Chen, Z. Liang, Y. Yang, C. Zhang, J. Yao and X. Wang, Tandem Catalysts Enabling Efficient C–N Coupling toward the Electrosynthesis of Urea, *Angew. Chem., Int. Ed.*, 2024, **63**(23), e202402215, DOI: 10.1002/anie.202402215.

9 J. Mukherjee, S. Paul, A. Adalder, S. Kapse, R. Thapa, S. Mandal, B. Ghorai, S. Sarkar and U. K. Ghorai, Understanding the Site-Selective Electrocatalytic Co-Reduction Mechanism for Green Urea Synthesis Using Copper Phthalocyanine Nanotubes, *Adv. Funct. Mater.*, 2022, **32**(31), 2200882, DOI: 10.1002/adfm.202200882.

10 B. Qiao, A. Wang, X. Yang, L. F. Allard, Z. Jiang, Y. Cui, J. Liu, J. Li and T. Zhang, Single-Atom Catalysis of CO Oxidation Using Pt1/FeOx, *Nat. Chem.*, 2011, **3**(8), 634–641, DOI: 10.1038/nchem.1095.

11 F. Ullah, K. Ayub and T. Mahmood, High Performance SACs for HER Process Using Late First-Row Transition Metals Anchored on Graphyne Support: A DFT Insight, *Int. J. Hydrogen Energy*, 2021, **46**(76), 37814–37823, DOI: 10.1016/j.ijhydene.2021.09.063.

12 T. He, C. Zhang and A. Du, Single-Atom Supported on Graphene Grain Boundary as an Efficient Electrocatalyst for Hydrogen Evolution Reaction, *Chem. Eng. Sci.*, 2019, 58–63, DOI: 10.1016/j.ces.2018.03.028.

13 L. Zong, K. Fan, W. Wu, L. Cui, L. Zhang, B. Johannessen, D. Qi, H. Yin, Y. Wang, P. Liu, L. Wang and H. Zhao, Anchoring Single Copper Atoms to Microporous Carbon Spheres as High-Performance Electrocatalyst for Oxygen Reduction Reaction, *Adv. Funct. Mater.*, 2021, **31**(41), 2104864, DOI: 10.1002/adfm.202104864.

14 L. Yang, D. Cheng, H. Xu, X. Zeng, X. Wan, J. Shui, Z. Xiang and D. Cao, Unveiling the High-Activity Origin of Single-Atom Iron Catalysts for Oxygen Reduction Reaction, *Proc. Natl. Acad. Sci. U. S. A.*, 2018, **115**(26), 6626–6631, DOI: 10.1073/pnas.1800771115.

15 H. Niu, X. Wang, C. Shao, Y. Liu, Z. Zhang and Y. Guo, Revealing the Oxygen Reduction Reaction Activity Origin of Single Atoms Supported on G-C3N4 Monolayers: A First-Principles Study, *J. Mater. Chem. A*, 2020, **8**(14), 6555–6563, DOI: 10.1039/d0ta00794c.

16 S. Kapse, S. Narasimhan and R. Thapa, Descriptors and Graphical Construction for in Silico Design of Efficient and Selective Single Atom Catalysts for the ENRR, *Chem. Sci.*, 2022, **13**(34), 10003–10010, DOI: 10.1039/d2sc02625b.

17 R. Thapa, N. Barman and S. Kapse, Electronic Descriptor to Identify the Activity of SACs for E-NRR and Effect of BF3 as Electrolyte Ion, *ChemSusChem*, 2024, **18**(2), e202400902, DOI: 10.1002/cssc.202400902.

18 K. Liu, J. Fu, L. Zhu, X. Zhang, H. Li, H. Liu, J. Hu and M. Liu, Single-Atom Transition Metals Supported on Black

 

Phosphorene for Electrochemical Nitrogen Reduction, *Nanoscale*, 2020, **12**(8), 4903–4908, DOI: 10.1039/c9nr09117c.

19 Z. Liu, A. Ma, Z. Wang, Z. Ding, Y. S. Pang, G. Fan and H. Xu, Single-Atom Anchored on Curved Boron Nitride Fullerene Surface as Efficient Electrocatalyst for Carbon Dioxide Reduction, *Mol. Catal.*, 2024, **559**, 114040, DOI: 10.1016/j.mcat.2024.114040.

20 F. Xu, X. Wang, X. Liu, C. Li, G. Fan and H. Xu, Computational Screening of TMN4 Based Graphene-like BC6N for CO2 Electroreduction to C1 Hydrocarbon Products, *Mol. Catal.*, 2022, **530**, 112571, DOI: 10.1016/j.mcat.2022.112571.

21 Q. Chang, Y. Liu, J. H. Lee, D. Ologunagba, S. Hwang, Z. Xie, S. Kattel, J. H. Lee and J. G. Chen, Metal-Coordinated Phthalocyanines as Platform Molecules for Understanding Isolated Metal Sites in the Electrochemical Reduction of CO2, *J. Am. Chem. Soc.*, 2022, **144**(35), 16131–16138, DOI: 10.1021/jacs.2c06953.

22 T. Liu, G. Wang and X. Bao, Electrochemical CO2Reduction Reaction on 3d Transition Metal Single-Atom Catalysts Supported on Graphdiyne: A DFT Study, *J. Phys. Chem. C*, 2021, **125**(47), 26013–26020, DOI: 10.1021/acs.jpcc.1c07681.

23 Z. Wang, A. Ma, Z. Liu, Z. Ding, Y. Pang, G. Fan and H. Xu, Density Functional Theory Study of Transition Metal Dual-Atom Anchored Phthalocyanine as High-Performance Electrocatalysts for Carbon Dioxide Reduction Reaction, *Appl. Surf. Sci.*, 2024, **669**, 160532, DOI: 10.1016/j.apsusc.2024.160532.

24 M. Shibata and N. Furuya, Electrochemical Synthesis of Urea at Gas-Diffusion Electrodes Part VI. Simultaneous Reduction of Carbon Dioxide and Nitrite Ions with Various Metallophthalocyanine Catalysts, *J. Electroanal. Chem.*, 2001, **507**(1–2), 177–184, DOI: 10.1016/S0022-0728(01)00363-1, https://www.elsevier.com/locate/jelechem.

25 T. J. Lin, W. S. Chen, H. C. Li, C. Y. Chen, H. Choi, Y. Kwon and M. J. Cheng, Metal-N4-Functionalized Graphene as Highly Active Catalysts for C-N Bond Formation in Electrochemical Urea Synthesis, *J. Phys. Chem. C*, 2025, **129**(7), 3424–3436, DOI: 10.1021/acs.jpcc.4c07971.

26 M. Shibata and N. Furuya, Electrochemical Synthesis of Urea at Gas-Diffusion Electrodes Part VI. Simultaneous Reduction of Carbon Dioxide and Nitrite Ions with Various Metallophthalocyanine Catalysts, *J. Electroanal. Chem.*, 2001, **507**, 177–184, DOI: 10.1016/S0022-0728(01)00363-1, https://www.elsevier.com/locate/jelechem.

27 Y. Huang, T. Fan and Y. Ji, Are Transition Metal Phthalocyanines Active for Urea Synthesis via Electrocatalytic Coupling of CO2 and N2?, *Phys. Chem. Chem. Phys.*, 2025, **27**, 531–538, DOI: 10.1039/d4cp04047c.

28 F. H. B. Lima, J. Zhang, M. H. Shao, K. Sasaki, M. B. Vukmirovic, E. A. Ticianelli and R. R. Adzic, Catalytic Activity - d-Band Center Correlation for the O2 Reduction Reaction on Platinum in Alkaline Solutions, *J. Phys. Chem. C*, 2007, **111**(1), 404–410, DOI: 10.1021/jp065181r.

29 D-Band_position.

30 J. Zhang, H. Jin, M. B. Sullivan, F. C. H. Lim and P. Wu, Study of Pd-Au Bimetallic Catalysts for CO Oxidation Reaction by DFT Calculations, *Phys. Chem. Chem. Phys.*, 2009, **11**(9), 1441–1446, DOI: 10.1039/b814647k.

31 G. Zhan, Y. Yao, F. Quan, H. Gu, X. Liu and L. Zhang, D-Band Frontier: A New Hydrogen Evolution Reaction Activity Descriptor of Pt Single-Atom Catalysts, *J. Energy Chem.*, 2022, **72**, 203–209, DOI: 10.1016/j.jechem.2022.05.012.

32 E. E. Siddharthan, S. Ghosh and R. Thapa, Site Specific Descriptors for Oxygen Evolution Reaction Activity on Single Atom Catalysts Using QMML, *J. Mater. Chem. A*, 2024, **12**(30), 19176–19186, DOI: 10.1039/d4ta02610a.

33 K. Liu, J. Fu, Y. Lin, T. Luo, G. Ni, H. Li, Z. Lin and M. Liu, Insights into the Activity of Single-Atom Fe-N-C Catalysts for Oxygen Reduction Reaction, *Nat. Commun.*, 2022, **13**(1), 2075, DOI: 10.1038/s41467-022-29797-1.

34 Y. Wang, Y. Liang, T. Bo, S. Meng and M. Liu, Orbital Dependence in Single-Atom Electrocatalytic Reactions, *J. Phys. Chem. Lett.*, 2022, **13**(25), 5969–5976, DOI: 10.1021/acs.jpclett.2c01381.

35 M. Shibata, K. Yoshida and N. Furuya, Electrochemical synthesis of urea on reduction of carbon dioxide with nitrate and nitrite ions using Cu-loaded gas-diffusion electrode, *J. Electroanal. Chem.*, 1995, **387**(1–2), 143–145, DOI: 10.1016/0022-0728(95)03992-P.

36 M. Shibata, K. Yoshida and N. Furuya, Electrochemical Synthesis of Urea at Gas-Diffusion Electrodes: IV. Simultaneous Reduction of Carbon Dioxide and Nitrate Ions with Various Metal Catalysts, *J. Electrochem. Soc.*, 1998, **145**, 2348, DOI: 10.1149/1.1838641.

37 M. Shibata, K. Yoshida and N. Furuya, Eleetrochemical Synthesis of Urea at Gas-diffusion Eleetrodes V. Simultaneous Reduction of Carbon Dioxide and Nitrite Ions with Various Boride Catalysts, *Denki Kagaku*, 1998, **66**(6), 584–589.

38 A. Biswas, S. Kapse, B. Ghosh, R. Thapa, R. Sundar Dey and Lewis, Acid-Dominated Aqueous Electrolyte Acting as Co-Catalyst and Overcoming $N_2$ Activation Issues on Catalyst Surface, *Proc. Natl. Acad. Sci. U. S. A.*, 2022, **119**(33), e2204638119, DOI: 10.1073/pnas.2204638119.

39 S. Paul, S. Sarkar, A. Adalder, S. Kapse, R. Thapa and U. K. Ghorai, Strengthening the Metal Center of Co-N4 Active Sites in a 1D-2D Heterostructure for Nitrate and Nitrogen Reduction Reaction to Ammonia, *ACS Sustain. Chem. Eng.*, 2023, **11**(16), 6191–6200, DOI: 10.1021/acssuschemeng.2c07114.

40 A. Adalder, S. Paul, N. Barman, A. Bera, S. Sarkar, N. Mukherjee, R. Thapa and U. K. Ghorai, Controlling the Metal-Ligand Coordination Environment of Manganese Phthalocyanine in 1D-2D Heterostructure for Enhancing Nitrate Reduction to Ammonia, *ACS Catal.*, 2023, **13**(20), 13516–13527, DOI: 10.1021/acscatal.3c02747.

41 B. B. Sarma, F. Maurer, D. E. Doronkin and J. D. Grunwaldt, Design of Single-Atom Catalysts and Tracking Their Fate Using Operando and Advanced X-Ray Spectroscopic Tools, *J. Am. Chem. Soc.*, 2023, **11**, 379–444, DOI: 10.1021/acs.chemrev.2c00495.

42 C. Ling, Y. Ouyang, Q. Li, X. Bai, X. Mao, A. Du and J. Wang, A General Two-Step Strategy–Based High-Throughput

Screening of Single Atom Catalysts for Nitrogen Fixation, *Small Methods*, 2019, **3**(9), 1800376, DOI: 10.1002/smtd.201800376.

43 S. Bhattacharjee, U. V. Waghmare and S. C. Lee, An Improved D-Band Model of the Catalytic Activity of Magnetic Transition Metal Surfaces, *Sci. Rep.*, 2016, **6**, 35916, DOI: 10.1038/srep35916.

44 E. Paquet and H. L. Viktor, Computational Methods for Ab Initio Molecular Dynamics, *Adv. Chem.*, 2018, **2018**, 1–14, DOI: 10.1155/2018/9839641.

45 A. Adalder, K. Mitra, N. Barman, R. Thapa, S. Bhowmick and U. K. Ghorai, Magneto-Electrochemical Ammonia Synthesis: Boosting Nitrite Reduction Activity by the Optimized Magnetic Field Induced Spin Polarized System, *Adv. Energy Mater.*, 2024, **14**(42), 2403295, DOI: 10.1002/aenm.202403295.

46 S. Kapse, N. Barman and R. Thapa, Identification of ORR Activity of Random Graphene-Based Systems Using the General Descriptor and Predictive Model Equation, *Carbon*, 2023, **201**, 703–711, DOI: 10.1016/j.carbon.2022.09.059.

47 C. Yates and D. J. Rlyholder, *I'iiper 1-38, I'roceedirlgs of the Third International Congress on Catalysis*, McQraw-Hill Rook Co., Inc, 1961, vol. 65.

48 Z. Fu, B. Yang and R. Wu, Understanding the Activity of Single-Atom Catalysis from Frontier Orbitals, *Phys. Rev. Lett.*, 2020, **125**(15), 156001, DOI: 10.1103/PhysRevLett.125.156001.

49 S. Maintz, V. L. Deringer, A. L. Tchougréeff and R. Dronskowski, LOBSTER: A Tool to Extract Chemical Bonding from Plane-Wave Based DFT, *J. Comput. Chem.*, 2016, **37**(11), 1030–1035, DOI: 10.1002/jcc.24300.

50 S. Maintz, V. L. Deringer, A. L. Tchougréeff and R. Dronskowski, Analytic Projection from Plane-Wave and PAW Wavefunctions and Application to Chemical-Bonding Analysis in Solids, *J. Comput. Chem.*, 2013, **34**(29), 2557–2567, DOI: 10.1002/jcc.23424.

51 V. L. Deringer, A. L. Tchougréeff and R. Dronskowski, Crystal Orbital Hamilton Population (COHP) Analysis as Projected from Plane-Wave Basis Sets, *J. Phys. Chem. A*, 2011, **115**(21), 5461–5466, DOI: 10.1021/jp202489s.